

# Reperfused Myocardial Infarction in Mice: 3D Mapping of Late Gadolinium Enhancement and Strain

Alistair A. Young, PhD,<sup>1</sup> Brent A. French, PhD,<sup>2</sup> Zequan Yang, MD, PhD,<sup>2</sup> Brett R. Cowan, MbChB,<sup>1</sup> Wesley D. Gilson, PhD,<sup>2</sup> Stuart S. Berr, PhD,<sup>2</sup> Christopher M. Kramer, MD,<sup>2</sup> and Frederick H. Epstein, PhD<sup>2</sup>

Faculty of Medical and Health Sciences, University of Auckland, Auckland, New Zealand<sup>1</sup>  
University of Virginia Health System, Charlottesville, Virginia, USA<sup>2</sup>

## ABSTRACT

We developed mathematical modeling tools for mapping 3D infarct geometry from multislice late gadolinium enhancement data, allowing fusion with multislice MR tagging data, in mice with myocardial infarction. Five C57BL/6 mice were imaged at baseline, 1, 7 and 28 days after 60 min occlusion of the left anterior descending coronary artery. The 3D infarct geometry was mapped in material coordinates, and registered with 3D strain, showing permanent dysfunction in infarcted segments, intermediate function in the adjacent zone, and maintained function in the remote zone. 3D mapping of late enhancement and strain allows registration of multiple studies in a consistent framework.

## INTRODUCTION

The mouse model of coronary occlusion is increasingly used to investigate both the genetics and pharmacologic therapy of left ventricular (LV) remodeling after myocardial infarction (MI). Transgenic and knockout mice are particularly useful in the study of the genetics of cardiovascular disease. The investigation of novel therapeutic strategies is also greatly facilitated by a murine model of reperfused MI. These studies require detailed phenotypic information, including regional ventricular shape and local myocardial function over a number of time points in the same animal. Magnetic resonance (MR)

imaging has been shown to produce accurate serial quantification of ventricular geometry with cine FLASH imaging (1), myocardial strain with MR tagging (2, 3), and infarction geometry with late gadolinium enhancement (2, 4) in murine models of MI.

However, the motion and myocardial strain patterns during the infarction and remodeling process are regionally heterogeneous, three-dimensional (3D), and dependent on the 3D infarct geometry. In order to quantify the 3D changes in myocardial strain after MI in relation to the infarct geometry, we extended and adapted a previously validated 3D analysis method (5) to perform serial, integrated analyses of 3D function and tissue characteristics in mice. We aimed, firstly, to develop tools for the regional analysis of 3D myocardial function in mice, secondly, to construct a 3D model of infarct geometry in relation to ventricular shape and motion, thirdly, to combine these data to determine 3D deformation parameters in infarcted and non-infarcted areas, and fourthly, to demonstrate the feasibility of these techniques in a murine model of reperfused MI over the first 28 days of LV remodeling.

## MATERIALS AND METHODS

This study conformed to the “Guide for the Care and Use of Laboratory Animals” published by the National Institutes of Health (NIH publication No. 85-23, revised 1985) and was conducted under protocols approved by the Institutional Animal Care and Use Committee at the University of Virginia.

*Keywords:* Ventricular Remodeling, Late Gadolinium Enhancement, Myocardial Strain, Data Fusion, Myocardial Infarction.

Received 5 January 2006; accepted 11 February 2006  
This work was supported by R01HL58582 (BAF), R01HL69696 (BAF), R01EB01763 (FHE), and the Health Research Council of New Zealand (AAY).

Correspondence to:

Alistair A. Young, PhD

Department of Anatomy with Radiology

Faculty of Medical and Health Sciences

University of Auckland

85 Park Rd, Grafton, Auckland

New Zealand

fax: +649 3737484

email: a.young@auckland.ac.nz

## ***Animal model***

MI was surgically induced in five C57BL/6 mice by 60 min occlusion of the left anterior descending (LAD) coronary artery followed by reperfusion (6). Mice were anesthetized, the upper portion of the trachea was exposed, and an endotracheal tube was inserted orally. Artificial respiration was maintained with an SAR-830/P ventilator (inspired oxygen fraction 0.80, rate 100 strokes/min, stroke volume 2.0–2.5 mL). After intubation, an incision was made to open the left pleural cavity. A 7-0 silk suture was passed underneath the LAD at the level of the lower left atrium and myocardial ischemia was induced by tying the suture over PE-10 tubing. After occlusion, reperfusion was achieved by removing the suture. Significant ECG changes (widening of the QRS wave and ST segment elevation as monitored with a PowerLab data recorder) and blanching within the region at risk were used to confirm coronary occlusion. A volume of 1–1.5 mL 5% dextrose was given intraperitoneally (i.p.) to replace fluids. Body temperature was maintained between 36.5–37.5°C with a heating pad during surgery. This protocol has been shown to reproducibly infarct the apex and antero-lateral midventricle (4).

## ***Cardiac MRI data acquisition***

The five mice were imaged at baseline, and at 1, 7 and 28 days after MI. For MR scanning, mice were anesthetized with isoflurane (1 vol. % in oxygen), pediatric electrocardiogram (ECG) leads (Blue Sensor, BRS-50-K/US, Ambu Inc., Linthicum, MD, USA) were attached to the two shaved forelimbs for ECG triggering, and temperature was maintained at  $37.0 \pm 0.5^\circ$  using circulating hot water. Core body temperature and ECG were monitored with an SAI Model 1025 monitoring and gating system (Small Animal Instruments, Inc., Stony Brook, NY, USA). A catheter was inserted in the peritoneal cavity for the i.p. infusion of gadolinium-DTPA (Magnevist, Schering AG, Berlin, Germany). MRI was performed on a 4.7T scanner (Varian, Inc., Palo Alto, CA, USA) using a custom-made birdcage RF coil (RF Design Consulting, Newberry, FL, USA) and gradients with a maximum strength of 80 G/cm and a slew rate of 66.7 G/cm/ms (Magnex Scientific, UK). The MR protocol included: 1) localizer scanning; 2) short-axis (6–8 slices) and long-axis (4 slices) imaging with black-blood myocardial tagging (7); and 3) for Day 1 studies, late gadolinium enhancement infarct imaging (6 slices).

All sequences used prospective ECG triggering, allowing imaging of 80–90% of the R-R interval. Short axis slices collected during the sequential imaging sequences had the same slice location, orientation, and FOV in order to enable direct comparison between the data sets. Temporal resolution was equal to TR (non-segmented acquisitions). All tagged images used a FLASH imaging sequence (1 mm slice thickness, 25.6 mm FOV,  $192 \times 96$  image matrix,  $20^\circ$  flip angle, TE 4.8 ms, TR 8.0–10.8 ms, 12 cardiac phases reconstructed) with a 6 lobe SPAMM preparation (4.8 ms duration) applied after the ECG trigger ( $180^\circ$  tag flip angle, 0.7 mm tag separation). The short axis images had two sets of tagged images acquired per slice (orthogonally oriented tags) with the higher-resolution readout

direction always perpendicular to the tag orientation (8). Long axis images had one set of tagged images per slice, with the tag orientation perpendicular to the left ventricular long axis.

Day 1 FLASH late gadolinium enhancement infarct imaging used 25.6 mm FOV,  $128 \times 128$  image matrix size, TE 3.2 ms and TR 100–130 ms. Six contiguous 1 mm thick short axis slices were obtained, covering the heart from the base to the apex, using a flip angle of  $60^\circ$  to increase the amount of T1 weighting. Three-tenths to six-tenths mmol/kg Gd-DTPA was infused i.p. after the tagged images, and the post-Gd images were acquired 15–30 min after injection to accurately measure infarct size (4, 9).

## ***LV geometry, mass and volume***

Figure 1 shows a flowchart of the data modeling and fusion process. Left ventricular geometry, mass and volume were determined from the black blood tagged cine images using guide point modeling (10) (Fig. 1, i–ii). Briefly, a “cardiac” coordinate system was constructed in relation to the canonical axes of the LV. The origin of this coordinate system was placed on the LV central axis one third of the distance from the base to the apex; the x axis was oriented toward the LV apex, the y axis was oriented towards the centroid of the right ventricle, and the z axis was oriented posteriorly. A 3D finite element model of the LV model was interactively manipulated using guide points placed by an experienced user so as to accurately model the shape of the ventricle. Anatomical markers located near the mitral valve and interventricular septum enabled accurate modeling of the 3D tilt and motion of the LV base, and registered the model with the cardiac anatomy. This method has been shown to produce efficient and accurate estimates of LV mass and volume (10). Relative positions around the heart could then be referenced by the finite element material coordinates. This allowed a non-rigid registration between studies, between both different acquisitions in the same animal, and different animals in a group, since regions with the same material coordinate denote the same physical region in the heart.

## ***Strain***

Image tags were tracked by an experienced user in each short and long axis image using a semi-automated active contour process, and the 3D motion was reconstructed with the aid of the finite element model, as described previously (5) (Fig. 1, iii–iv). This resulted in a dynamic model of the LV deformation. The Lagrangian Green strain components between end-diastole and each subsequent time were calculated at specific finite element material points using standard methods of continuum mechanics (11). Previous validation experiments using a deformable silicone gel phantom have shown that this procedure produces accurate, unbiased estimates of displacement and shortening (5).

The dynamic finite element model was divided into 16 standardized regional segments (12). The displacement and strain at material points corresponding to the tracked tags were averaged for each segment. Strain results were not obtained in the apical tip of the LV (region 17) due to partial volume effects in the short axis images.

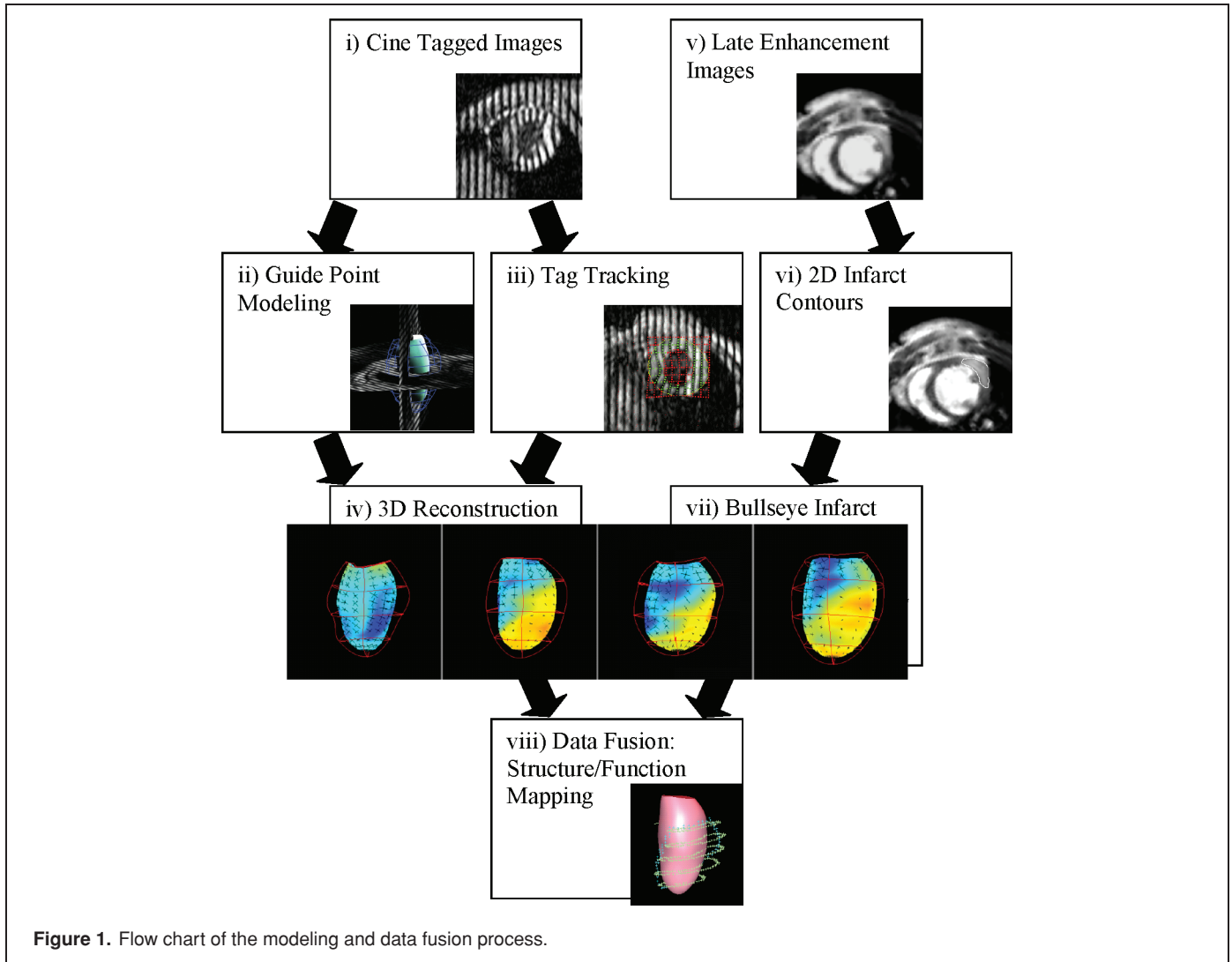


Figure 1. Flow chart of the modeling and data fusion process.

### Infarct geometry

Infarcted regions in the Day 1 late gadolinium enhancement images were outlined by an experienced user on each image in the short axis stack (Fig. 1, v–vi) using the ImageJ image analysis program (ImageJ, NIH, Bethesda, MD, USA) (13). The image coordinates of the contours were then transformed into 3D magnet coordinates using the 3D location of the image planes. The magnet coordinates were then transformed into the  $(x, y, z)$  cardiac coordinate system defined above. The cardiac coordinates of the contours were then converted to 3D spherical polar coordinates according to:

$$r = \sqrt{x^2 + y^2 + z^2}; \quad \theta = \tan^{-1} \left( \frac{z}{y} \right); \quad \mu = \cos^{-1} \left( \frac{x}{r} \right). \quad [1]$$

The 3D contour points were then mapped into a 2D bullseye projection map with coordinates  $(u, v)$  calculated from the spherical polar coordinates:

$$u = \mu \sin(\theta); \quad v = \mu \cos(\theta). \quad [2]$$

Viewed in the bullseye map, the hyperenhancement contours denote the extent of the infarct around the surface of the LV. A convex perimeter was manually drawn by the same user on the bullseye map so as to enclose the hyperenhancement contours in  $(u, v)$  space (Fig. 1, vii). The  $(u, v)$  coordinates of the perimeter were then converted to 3D polar coordinates and projected in the radial direction onto the midwall surface of the LV finite element model. This allowed the calculation of the 3D infarct geometry in finite element material coordinates. The 3D infarct geometry was fixed onto the dynamic finite element model at end-diastole, and allowed to deform with the beating model during systole and diastole (Fig. 1, viii).

Material points within the finite element model were assigned to regions relative to the 3D infarct geometry as follows: points within the 3D infarct geometry were denoted *infarct*, points within 1.0 mm of the 3D infarct geometry (but outside it) were denoted *adjacent*, and all other points were denoted *remote* (the 3D adjacent zone width of 1.0 mm was chosen to correspond to the 2D characterization used in Reference 2. This procedure also allowed calculation of the percentage myocardium in the

infarct and adjacent and remote zones, respectively. Since the models were defined in a coordinate system aligned with each heart, a material point could be mapped onto the corresponding material point at each timepoint during remodeling. The material points of the 3D infarct geometry at Day 1 could thus be mapped into the baseline, and Day 7 and Day 28 models to give an approximate corresponding region for comparison purposes (Fig. 1, viii).

### Statistics

Data were analyzed using the Statistica software package (version 6.1, Statsoft, Tulsa, OK, USA). All data are presented as means  $\pm$  SEM. Repeated measures ANOVA were performed to test for differences in mass, volumes and heart rate and the Dunnett post hoc test used to test differences from baseline.

Strains at all tracked tag points were averaged into the 16 standard LV myocardial segments. To test for segmental differences in the longitudinal direction of the LV, repeated measures ANOVA was performed for three longitudinal levels (apex, mid-ventricle, and base, each averaged over all circumferential segments) and four timepoints (baseline, Day 1, Day 7 and Day 28). Similarly, to test for circumferential differences, repeated measures ANOVA was performed for four circumferential levels (septal, posterior, lateral, and anterior, each averaged over all longitudinal segments) and four time points. Scheffé post hoc tests were used to test for regional differences due to timepoint in each case.

Strains were also averaged in remote, adjacent and infarct regions, and repeated measures ANOVA was performed to test

**Table 1.** LV mass and volumes, mean  $\pm$  SEM (n = 5) at the four time points.

	Mass(mg)	EDV( $\mu$ L)	ESV( $\mu$ L)	SV( $\mu$ L)	EF(%)	HR (bpm)
Baseline	95 $\pm$ 3	45 $\pm$ 3	18 $\pm$ 1	27 $\pm$ 2	59 $\pm$ 2	406 $\pm$ 17
Day 1	103 $\pm$ 4	45 $\pm$ 2	28 $\pm$ 2*	17 $\pm$ 1*	38 $\pm$ 3*	489 $\pm$ 51*
Day 7	102 $\pm$ 3	61 $\pm$ 4*	40 $\pm$ 4*	21 $\pm$ 2	34 $\pm$ 3*	431 $\pm$ 16
Day 28	118 $\pm$ 6*	72 $\pm$ 4*	48 $\pm$ 6*	24 $\pm$ 4	34 $\pm$ 5*	430 $\pm$ 15

\*p < 0.05 vs baseline, Dunnett test.

differences due to timepoint. Scheffé post hoc tests were used to test for regional differences as above.

## RESULTS

### Mass, volume and heart rate

Table 1 shows mean mass, volume and heart rate results. Ejection fraction was reduced to 38% at Day 1 and remained impaired to Day 28. End-diastolic volume was unchanged at Day 1 but increased 60% by Day 28. End-systolic volume also increased with time to Day 28. Stroke volume was decreased at Day 1 but normalized by Day 28. Heart rate was increased at Day 1 and normalized by Day 7 and Day 28.

### Strain

Figure 2 shows typical SPAMM tagged images for a study at baseline and at Day 1. Due to the high heart rate in mice, there was minimal tag fading through the cardiac cycle, allowing all tags to be tracked throughout the 12 frames acquired.

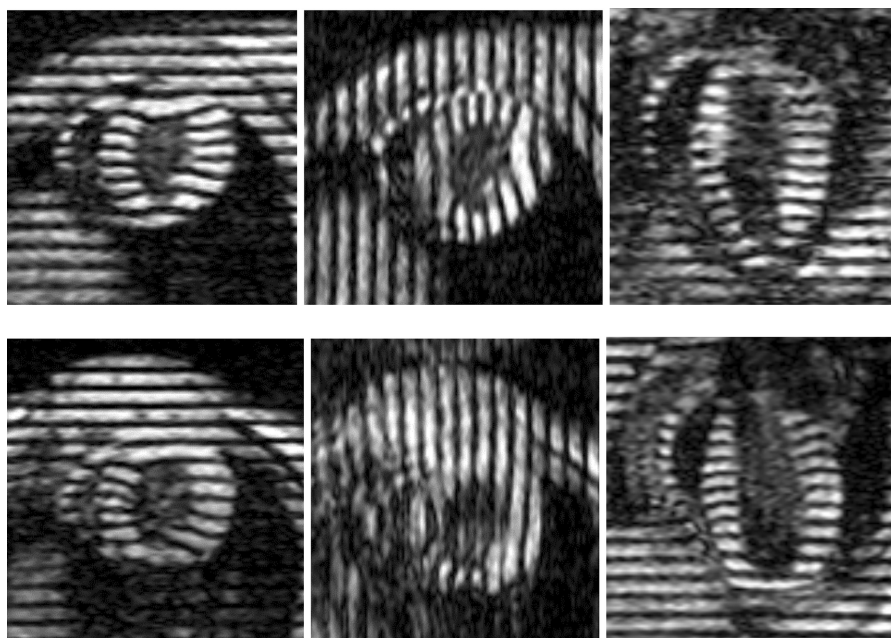


**Figure 2.** SPAMM tagged MR images for one mouse, at baseline (top) and Day 1 after MI (bottom). The left column shows short-axis midventricular slices with horizontal tags, middle column shows the same short-axis slices with vertical tags, and the right column shows a long axis slice. SPAMM stripes in the chest wall are 0.7 mm apart.

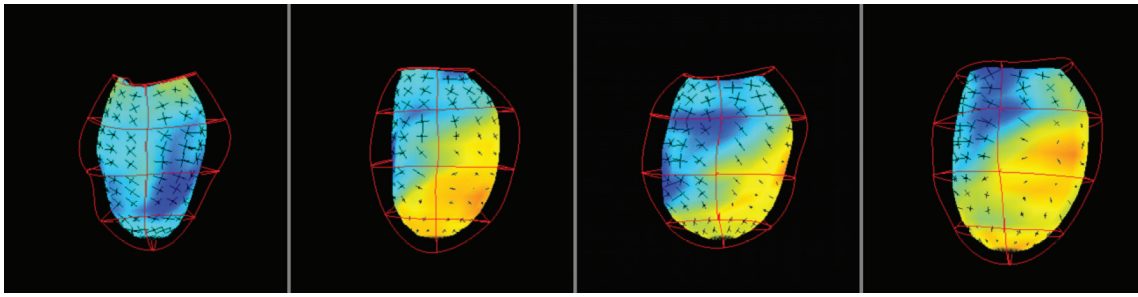


**Figure 3.** Three-dimensional finite element model at end systole, at baseline, and at Day 1, Day 7 and Day 28 post-MI (left to right, respectively) in the same mouse as Fig. 2. The septum is on the left. Lines denote model element boundaries. Crosses denote 3D principal strains and directions.

Figure 3 shows 3D principal strains rendered on the midwall surface of the FE model at baseline, Day 1, Day 7 and Day 28 for a typical case. The material boundaries of the region of impaired function were consistent throughout the remodeling process. Infarcted regions showed a pronounced deficit in function throughout the 28 day remodeling period.

Circumferential strain in the 16 standard regions is shown in Fig. 4a. The apex and midventricle levels were significantly reduced at Day 1, Day 7 and Day 28 ( $p < 0.01$ ), whereas the base level was not ( $p = \text{NS}$ ). The posterior, anterior and lateral segments were reduced at Day 1, Day 7 and Day 28 ( $p < 0.01$ ), whereas the septum was not significantly different from baseline at any stage.

Longitudinal strain (Fig. 4b) showed similar patterns to circumferential strain. The apex and midventricle levels were significantly reduced at all stages of MI ( $p < 0.01$ ), whereas the base level was not ( $p = \text{NS}$ ). The anterior and lateral segments were impaired at all stages after MI ( $p < 0.01$ ); the posterior segment was only significantly different from baseline at Day 28 ( $p < 0.01$ ); the septum was not significantly different from baseline at any stage.

The 3D principal shortening strain is shown in Fig. 4c. This is the maximal contraction (in any direction) at a given point and typically occurs in a direction which is not aligned with any image plane. The maximal contraction can thus be viewed as a 3D combination of circumferential and longitudinal shortening as well as ventricular torsion. Similar patterns to the circumferential and longitudinal strains were therefore observed. The 3D principal shortening strain in the apex and midventricle levels showed marked reduction at all stages after MI ( $p < 0.01$ ), whereas the base was not significantly effected. The posterior, lateral and anterior walls showed marked reduction at all stages after MI ( $p < 0.01$ ); however, the septum maintained function at all time points.

### Infarct geometry

Figure 5 shows late gadolinium enhanced images for a typical Day 1 study. Clear regions of hyperenhancement could be delineated in each slice and projected onto the bullseye map (Fig. 6a). The convex perimeter enclosing the projected hyperenhancement contours were drawn manually on the  $u$ - and  $v$ -space map

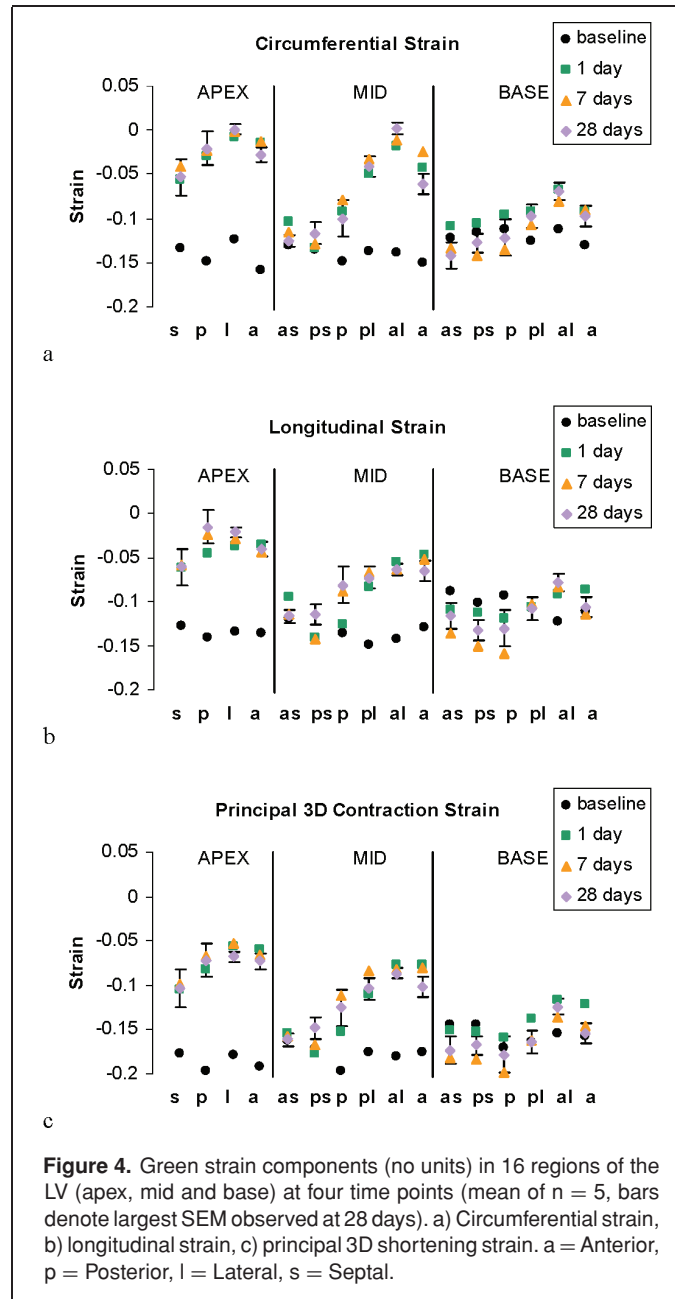


**Figure 4.** Green strain components (no units) in 16 regions of the LV (apex, mid and base) at four time points (mean of  $n = 5$ , bars denote largest SEM observed at 28 days). a) Circumferential strain, b) longitudinal strain, c) principal 3D shortening strain. a = Anterior, p = Posterior, l = Lateral, s = Septal.

## DISCUSSION

Cardiac MRI has several advantages in the study of reperfused myocardial infarction in mice. Firstly, it is not limited in the coverage of the heart, has good contrast to noise ratio, and requires no simplifying assumptions in the calculation of geometry, mass and volume. Secondly, accurate and precise estimates of myocardial strain can be performed with MR tagging or related displacement encoding techniques (2, 3, 15). Thirdly, late gadolinium enhancement imaging allows precise definition of the region of infarction and has shown excellent agreement with the histological area of necrosis in dogs (16), rats (9) and mice (4). The current study demonstrates the feasibility of integrating these three techniques into a comprehensive 3D analysis of myocardial structure and function.

The feasibility of the data fusion method was investigated in the context of post-infarction LV remodeling in mice. Since each separate technique has been previously validated, including infarct size determination, strain measurement, and geometric modeling (2–5, 9, 10, 14–16), we did not perform additional validation of these techniques in this study. The 3D strain analysis and guide point modeling methods, previously validated in humans and phantom (5, 10), was applied to mice without significant modification since the relative resolution and contrast to noise ratio are comparable to human imaging (1–4). In the following sections we compare the results with previous studies using the same murine model.

The mouse model of prolonged LAD occlusion followed by reperfusion was chosen because it yields a reproducibly large MI, and mimics the standard clinical practice of reperfusion by direct angioplasty or thrombolytics. In a previous study of MI in mice after 1 or 2 hour LAD occlusion and reperfusion, multi-slice anatomical cine imaging showed greater than 50% reduction in ejection fraction, which was maintained throughout the remodeling process (1). LV end-systolic volume increased three-fold, and end-diastolic volume increased two-fold by 4 weeks

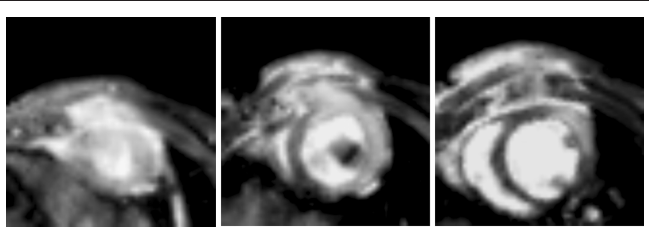


**Figure 5.** Late gadolinium enhancement images showing apical (left), midventricle (middle) and basal (right) short axis slices (same case as in Fig. 2).

as shown in Fig. 6a. The convex perimeter was then projected onto the 3D model to construct a material infarct boundary as shown in Fig. 6b. The 3D strain map could then be viewed in relation to the material infarct boundary (Fig. 6c).

The material points of the LV FE model were divided into infarct, adjacent and remote regions as defined above. The mean percentage total myocardium in the infarct, adjacent and remote zones was  $40 \pm 2\%$ ,  $29 \pm 1\%$ , and  $31 \pm 3\%$ , respectively. Figure 7 shows the circumferential, longitudinal and principal strain in these regions at all time points. The circumferential strain (Fig. 7a) was essentially nil post MI in the infarct zone ( $p < 0.01$  for Days 1, 7 and 28); the adjacent zone showed reduced function at all time points after MI ( $p < 0.01$ ) whereas the remote zone was not significantly changed. The longitudinal strain (Fig. 7b) showed reductions in the infarct and adjacent zones ( $p < 0.01$ ) with the exception of the adjacent zone at Day 1 ( $p = 0.08$ ). Longitudinal strain in the remote zone was not significantly changed at Day 1 and Day 28 but was significantly increased at Day 7 ( $p = 0.03$ ). Torsional shear strain (associated with ventricular twist) was significantly reduced in the infarct zone at Day 28 only, with no other significant changes. The 3D principal strain (Fig. 7c) showed decreased function in the infarct and adjacent zones ( $p < 0.01$ ).

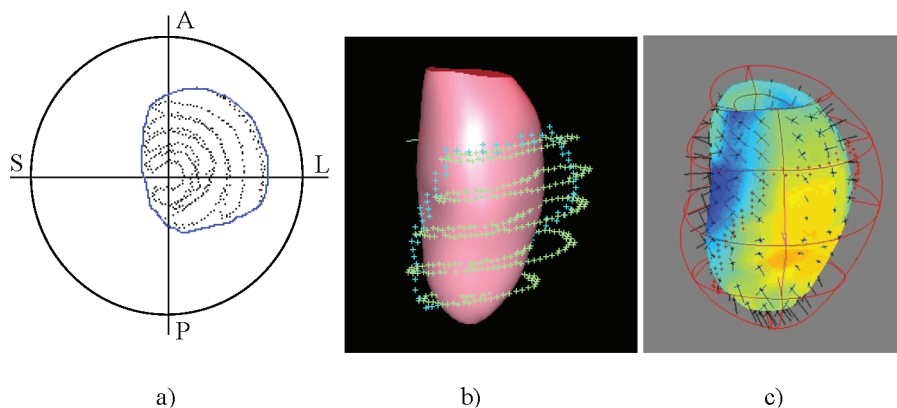
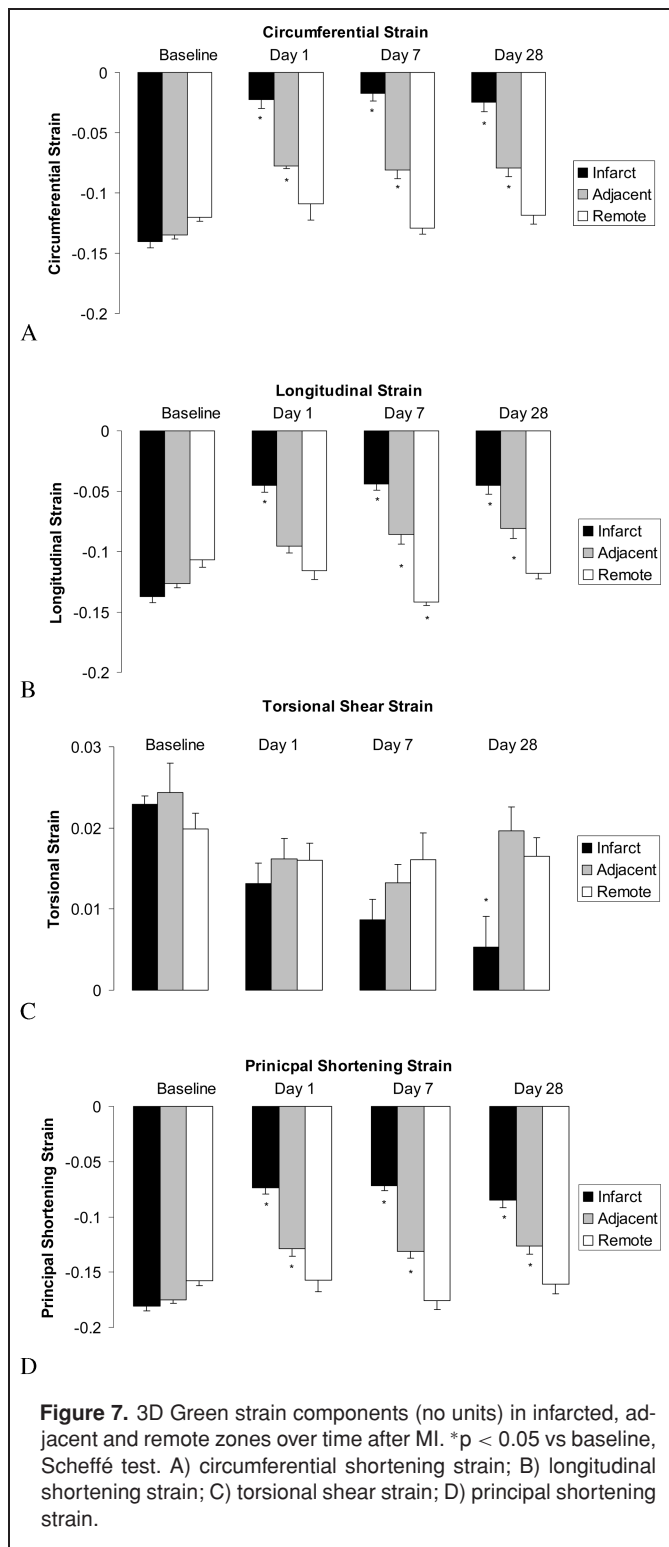


**Figure 6.** a) Late gadolinium enhancement contours (black dots) projected into the  $(u, v)$  bullseye map (same mouse as Fig. 5). The LV apex  $(u, v) = (0, 0)$  is the middle of the plot; outer circle denotes LV base. Convex perimeter enclosing the hyperenhancement contours is shown as a solid line. b) Finite element model (endocardial surface shaded) with hyperenhancement contours (green crosses) and 3D infarct boundary (cyan crosses). c) Strain map at midwall in relation to 3D infarct boundary; shading denotes maximal shortening (blue  $-0.2$ , red  $0.0$ ) (See online for color version). A: anterior; S: septal; P: posterior; L: lateral.



post-MI (1). These results, obtained with traditional slice summation methods, are similar to the results of the present study obtained with 3D guide point modeling. Also, the heart rate during MR imaging was similar to that reported by previous studies (4, 15) with a similar increase in heart rate at Day 1 observed by Yang et al. (4).

Previous studies of late enhancement imaging of reperfused myocardial infarction in mice have shown excellent agreement with histological staining by TTC (4). Areas of hyperenhancement in apical, midventricle and basal slices were similar to those observed by Gilson et al. (15).

Epstein et al. (2) quantified local 2D circumferential shortening in the imaging plane in 8 C57BL/6 mice before and after MI. Late gadolinium enhancement imaging was used to determine infarcted, adjacent and remote zones. At Day 1, a decrease was found in circumferential 2D shortening from 14.5% at baseline to 0.7% in the infarct zone, 7.4% in the adjacent zone and 11.8% in the remote zone, similar to the results of the current study. The values of circumferential shortening found in the current study are also similar to those found by Zhou et al. (3), who quantified global and regional strain using SPAMM tagging, and Gilson et al. (15), who used DENSE imaging at baseline and Day 1.

The longitudinal shortening patterns were similar to the circumferential direction, except for the finding of increased function in the remote zone at Day 7 after MI. This requires further study, one possible mechanism being compensatory augmentation prior to the completion of LV remodeling. Longitudinal function may be a sensitive index of LV function in mice (15) and humans (17, 18).

Torsion was quantified in normal mice using SPAMM tagging by Henson et al. (19) and Zhou et al. (3) and using 3D DENSE by Gilson et al. (15). The baseline values of torsion are similar in mice and humans, using similar methodology. A reduction in torsion was observed at Day 1 using 3D DENSE (15). In the current study, the reduction in torsion in the infarct zone was progressive with time, becoming significant at Day 28.

### Limitations

Limitations of this study include the labor intensive nature of the tag analysis and late gadolinium enhancement contour identification. Automation of these processes is an active area of research.

Gadolinium enhanced imaging in mice is challenging at Days 7 and 28 post-MI due to reduced enhancement and wall thinning. In the current study, we therefore mapped the material infarct geometry between imaging timepoints using the registration provided by the LV model. More accurate 3D infarct geometry imaging can be achieved using an inversion recovery contrast enhanced technique (20), and an inversion recovery technique for delayed contrast enhanced imaging at all timepoints after MI in mice has subsequently been developed (21).

The bullseye plot 3D infarct mapping method employed in this work assumes a fully transmural infarct incorporating the LV apex. This is typical for the reperfused mouse infarct model used in this study. An extension to non-transmural infarcts or arbitrary geometry is possible by using a 3D surface enclosing the image hyperenhancement contours.

A limitation of SPAMM tagging is that the resolution of strain measurement is low relative to the resolution of the images, due to the tag spacing, and some variation in the adjacent zone may be missed. However, higher resolution 3D strain imaging

is possible with DENSE imaging (15, 22), and the techniques developed in this study are directly applicable to DENSE data analysis.

## CONCLUSIONS

This study demonstrates how 3D analyses of myocardial infarction from multislice late gadolinium enhancement imaging can be combined with 3D strain information from multislice MR tagging and applied in mice to study LV dysfunction post-MI. Results of the 3D analysis extend 2D findings previously described in mice. These quantitative tools will be useful in determining the effects of genetic manipulation and/or pharmacologic therapy on LV remodeling. In addition, these tools can be applied to the analysis of diastolic function in a straightforward manner, since tags are easily tracked throughout diastole as well as systole.

## REFERENCES

1. Ross AJ, Yang Z, Berr SS, Gilson WD, Petersen WC, Oshinski JN, French BA. Serial MRI evaluation of cardiac structure and function in mice after reperused myocardial infarction. *Magn Reson Med* 2002;47:1158–68.
2. Epstein FH, Yang Z, Gilson WD, Berr SS, Kramer CM, French BA. MR tagging early after myocardial infarction in mice demonstrates contractile dysfunction in adjacent and remote regions. *Magn Reson Med* 2002;48:399–403.
3. Zhou R, Pickup S, Glickson JD, Scott CH, Ferrari VA. Assessment of global and regional myocardial function in the mouse using cine and tagged MRI. *Magn Reson Med* 2003;49:760–64.
4. Yang Z, Berr SS, Gilson WD, Toufektsian M-C, French BA. Simultaneous evaluation of infarct size and cardiac function in intact mice by contrast-enhanced cardiac magnetic resonance imaging reveals contractile dysfunction in noninfarcted regions early after myocardial infarction. *Circulation* 2004;109:1161–7.
5. Young AA, Kraitchman DL, Dougherty L, Axel L. Tracking and finite element analysis of stripe deformation in magnetic resonance tagging. *IEEE Trans Medical Imaging* 1995;14:413–21.
6. Yang Z, Bove CM, French BA, Epstein FH, Berr SS, DiMaria JM, Gibson JJ, Carey RM, Kramer CM. Angiotensin II type 2 receptor overexpression preserves left ventricular function after myocardial infarction. *Circulation* 2002;106:106–11.
7. Berr SS, Roy, French BA, Yang Z, Gilson WD, Kramer CM, Epstein FH. Black blood gradient echo cine magnetic resonance imaging of the mouse. *Magn Reson Med* 2005;53:1074–9.
8. McVeigh ER. MRI of myocardial function: motion tracking techniques. *Magn Reson Imaging* 1996;14:137–50.
9. Oshinski JN, Yang Z, Jones JR, Mata JF, French BA. Imaging time after Gd-DTPA is critical in using delayed enhancement to determine infarct size accurately with MRI. *Circulation* 2001;104:2838–42.
10. Young AA, Cowan BR, Thrupp SF, Hedley WJ, Dell'Italia LJ. Left ventricular mass and volume: Fast calculation with guide-point modeling on MR images. *Radiology* 2000;216(2):597–602.
11. Fung YC. *Foundations of Solid Mechanics*. Prentice Hall, London, pp 97.
12. Cerqueira MD, Weissman NJ, Dilsizian V, Jacobs AK, Kaul S, Laskey WK, Pennell DJ, Rumberger JA, Ryan T, Verani MS. Standardized myocardial segmentation and nomenclature for tomographic imaging of the heart: a statement for healthcare professionals from the Cardiac Imaging Committee of the Council on Clinical Cardiology of the American Heart Association. *Circulation* 2002;105(4):539–42.
13. Rasband WS, ImageJ, U.S. National Institutes of Health. Available at: <http://rsb.info.nih.gov/ij/>. Accessed 10 May 2006.
14. Ruff J, Wiesmann F, Hiller KH, Voll S, von Kienlin M, Bauer WR, Rommel E, Neubauer S, Haase A. Magnetic resonance microimaging for noninvasive quantification of myocardial function and mass in the mouse. *Magn Reson Med* 1998;40:43–8.
15. Gilson WD, Yang Z, French BA, Epstein FH. Measurement of myocardial mechanics in mice before and after infarction using multislice displacement-encoded MRI with 3D motion encoding. *Am J Physiol Heart Circ Physiol* 2005;288:H1491–7.
16. Kim RJ, Fieno DS, Parrish TB, Harris K, Chen EL, Simonetti O, Bundy J, Finn JP, Klocke FJ, Judd RM. Relationship of MRI delayed contrast enhancement to reversible injury, infarct age, and contractile function. *Circulation* 1999;100:1992–2002.
17. Yu CM, Lin H, Yang H, Kong SL, Zhang Q, Lee SW. Progression of systolic abnormalities in patients with “isolated” diastolic heart failure and diastolic dysfunction. *Circulation* 2002;105:1195–201.
18. Rydberg E, Gudmundsson P, Kennedy L, Erhardt L, Willenheimer R. Left atrioventricular plane displacement but not left ventricular ejection fraction is influenced by the degree of aortic stenosis. *Heart* 2004;90:1151–5.
19. Henson RE, Song SK, Pastorek JS, Ackerman JJ, Lorenz CH. Left ventricular torsion is equal in mice and humans. *Am J Physiol Heart Circ Physiol* 2000;278:H1117–23.
20. Simonetti OP, Kim RJ, Fieno DS, Hillenbrand HB, Wu E, Bundy JM, Finn JP, Judd RM. An improved MR imaging technique for the visualization of myocardial infarction. *Radiology* 2001;218:215–23.
21. French BA, Beyers RJ, Florent C, Sureau MS, Yang Z, Gilson WD, Roy J, Berr SS, Epstein FH. Imaging infarct expansion in mice using a contrast-enhanced inversion recovery MRI sequence. *J Cardiovasc Magn Reson* 2005;7:172.
22. Kim D, Gilson WD, Kramer CM, Epstein FH. High-resolution myocardial tissue tracking with two-dimensional cine displacement-encoded MRI. *Radiology* 2002;230:862–71.